CI&CEQ
Chemical Industry & Chemical Engineering Quarterly

Available on line at
Association of the Chemical Engineers of Serbia AChE
www.ache.org.rs/CICEQ

Chem. Ind. Chem. Eng. Q. 20 (2) 249–260 (2014) CI&CEQ

HUA-RONG LI[1]
LIMING CHE[1]
ZHENG-HONG LUO[1,2]

[1]Department of Chemical and Biochemical Engineering, Xiamen University, Xiamen, China
[2]Department of Chemical Engineering, Shanghai Jiao Tong University, Shanghai, China

SCIENTIFIC PAPER

UDC 678.742.3:66.095.26:544

DOI 10.2298/CICEQ120722006L

MODELING INTRAPARTICLE TRANSPORTS DURING PROPYLENE POLYMERIZATIONS USING SUPPORTED METALLOCENE AND DUAL FUNCTION METALLOCENE AS CATALYSTS: SINGLE PARTICLE MODEL

Article Highlights

- We suggest two improved multigrain models
- Propylene polymerization with silica-supported metallocene catalyst is simulated
- Propylene polymerization with silica-supported dual function metallocene catalyst is simulated
- The two propylene polymerizations are compared numerically

Abstract

Two improved multigrain models (MGMs) for preparing homopolypropylene and long chain branched polypropylene via propylene polymerization using silica-supported metallocene or dual function metallocene as catalysts are presented in this paper. The presented models are used to predict the intra-particle flow fields involved in the polymerizations. The simulation results show that the flow field distributions involved are basically identical. The results also show that both polymerization processes have an initiation stage and the controlling step is reaction-diffusion-reaction with the polymerization proceeding. Furthermore, the simulation results show that the intraparticle mass transfer resistance has significant effect on the polymerization, but the heat transfer resistance can be ignored.

Keywords: şilica-supported metallocene catalyst, silica-supported dual function metallocene catalyst, shell-by-shell fragmentation, propylene polymerization, long chain branched polyolefins, particle growth model.

High catalyst activity and synthetic accessibility of tailor-made polymers with well-defined microstructures and narrow molar mass distributions represent the main advantages of metallocene catalysts in comparison to Ziegler-Natta or Phillips catalysts [1]. Metallocene catalysts have recently become increasingly important as versatile transition metal catalysts for olefin polymerization and are used to prepare abundant polyolefins including linear and long chain-branched polyolefins (LCBPs) [2,3]. The LCBPs are prepared using constrained-geometry catalyst (CGC) and metallocene catalyst (a dual function metallocene catalyst) simultaneously [4-6]. The presence of LCBs alters the viscoelastic properties of these resins [7] to result in better rheological properties. When these metallocene catalysts are used as homogeneous catalysts in the plant, they are immobilized on the surface of a solid carrier [8]. The major objective of catalyst immobilization is to preserve the advantages of a homogeneous catalyst and at the same time to provide acceptable polymer particle morphology. Controlled fragmentation of the initial supporting particles is thus very important here. In addition, immobilization increases the complexity of metallocene--catalyzed systems [9]. Amorphous SiO_2 has generally been the preferred support for metallocene immobilization. Silica is used to control the morphology of the polymer, and its unique surface chemistry can be used to immobilize reagents [10].

During the polymerization over SiO_2-supported metallocene catalyst, the polymer formed inside the

Correspondence: Z.-H. Luo, Department of Chemical and Biochemical Engineering, Xiamen University, Xiamen 361005, P. R. China.
E-mail: luozh@xmu.edu.cn
Paper received: 22 July, 2012
Paper revised: 15 January, 2013
Paper accepted: 4 February, 2013

catalyst pores at the very early stage of polymerization results in catalyst fragmentation and the formation of a large number of microparticles. As the reaction proceeds, the catalyst microparticles are encapsulated by the growing polymer chains, leading to the formation of a pseudohomogeneous polymer macroparticle and a decrease in particle porosity [11]. Meanwhile, the catalyst fragmentation and the intraparticle mass and heat transfer involved may change the polymerization kinetics and then influence the final polymer performances [11]. Therefore, intraparticle mass and heat transfer models is useful for better understanding the propylene polymerization over supported metallocene catalysts and dual function catalysts.

In order to study intraparticle mass and heat transfer, mass and energy balance equations for particle growth have to be solved. So far, four single particle models [10], namely, the solid core model (SCM) [12], polymeric flow model (PFM) [13], multigrain particle model (MGM) [14], and polymeric multigrain model (PMGM) [15], have been widely used to describe the particle growth in olefin polymerization. Due to the complete transient fragmentation of heterogeneous Ziegler-Natta catalysts, the single-particle models mentioned above have been used mainly for modeling heterogeneous Ziegler-Natta olefin polymerization [10]. However, microscopic analysis of SiO_2 supported metallocene catalysts has shown that the fragmentation mechanism of SiO_2 particles during polymerization is shell-by-shell fragmentation of the particle from the surface to the core [11,16–25]. Therefore, the models mentioned above can not be employed in the olefin polymerization over supported metallocene catalysts directly. For instance, Boninii *et al.* [16] proved that the MGM could not fit experimental data involving gradual particle fragmentation. Then they developed a “particle growth model” for silica supported metallocene catalysts, which was based on the same ideas of MGM but assumed a gradual fragmentation of the particle. In this way, the particle was divided into two distinct parts: a fragmented (which behaves exactly like in the MGM) and an unfragmented one. However, the unfragmented core was not modeled properly and diffusion or polymerization inside the core is basically ignored in the Boninii *et al.* model [16]. Alexiadis *et al.* [17,18] proposed a more general approach derived directly from the Bonini *et al.* model but with the addition of a further part regarding the unfragmented core. In the model by Alexiadis *et al.* two kinds of particles are identifiable: macroparticles (the original pellet) and microparticles (the resulted fragments). Diffusion of monomer into the fragmented part is a two-step process. The monomer diffuses into the macroparticle (macro-scale) first, and then diffuses into the polymeric layer of the microparticle (micro-scale). Finally, it reaches the catalytic active sites and begins to react (molecular scale). Diffusion and reaction in the unfragmented core, on the other hand, is simpler because there are no microparticles and only two scales are involved. This model overcomes some of the limitations of the Boninii *et al.* model and can predict the initial peak, which appears in the reaction rate profile. Nevertheless, the catalyst deactivation and the concentration transition between fragmented and unfragmented parts in macroparticle were still ignored in the Alexiadis *et al.* model. In addition, in most of the single particle models involving the SiO_2 supported metallocene catalyst, the energy balance equations for particle growth were ignored. Furthermore, no open models deal with supported dual function metallocene catalysts for preparing LCBPs as far. On the other hand, Soares and Hamielec [26] suggested a dynamic mathematical model to describe homogeneous and heterogeneous Ziegler-Natta catalyzed copolymerizations with considering multiple catalytic site types and mass and heat transfer effects on polymerization rate and polymer properties. However, the mass and heat transfer belongs to external transfer instead of intraparticle transfer. In addition, soluble catalysts are regarded as a special case of the general modeling where only one or two site types are present and mass and heat transfer resistances are considered negligible.

In this work, two improved multigrain models (MGMs) are proposed to describe propylene polymerizations with SiO_2-supported metallocene catalyst and dual function metallocene catalyst to prepare homopolypropylene and LCB polypropylene. Different from previous models [11,16-26], the proposed models incorporate the energy balance equations for considering intraparticle heat transfer limitation, the catalyst deactivation and the concentration transition between fragmented and unfragmented parts in macroparticle. In addition, this work focuses on the comparison of intraparticle flow field using supported setallocene and dual function metallocene.

MODEL DEVELOPMENT

Physical model for particle evolution

Since the present work aims at suggesting two single particle models to predict and compare intraparticle flow fields in propylene polymerization over two types of SiO_2-supported metallocene catal-

ysts, physical models describing the evolution of these particles must be presented first. The metallocene catalysts mentioned above are all supported by SiO_2 particles, so the physical models for their evolutions are basically identical [11]. There are many published reports [11,16-25] on the fragmentation and evolution of SiO_2-supported metallocene catalysts and their evolution mechanism has been generally acknowledged [11]. Here, the acknowledged mechanism and corresponding physical model are adopted.

The morphological studies of catalyst systems at different time show that the particle growth starts right after the induction period and proceeds continually as the polymerization activity increases [11,16-20]. In polymerization, particles are considered to be spherical and fragmentation occurs shell-by-shell from the surface to centre. In this way, it is possible to identify two distinct regions: a fragmented shell and an unfragmented core (see Figure 1).

The particle is fragmenting and the fragmentation front is moving towards the centre of the particle. When the fragmentation front reaches the centre of the particle, the particle is assumed to be completely fragmented. The fragments are also assumed spherical as in the MGM. Based on the previous description and Figure 1, some points related to the following mathematical model are emphasized as follows.

First, in polymerization, the fragmentation occurs shell-by-shell from the surface to the centre of the catalyst-containing particles and two kinds of particles are identifiable: macro-particles and micro-particles.

Second, the polymerization process can be divided into two typical periods, *i.e.*, the periods without and with fragmentation. The one with fragmentation can be divided into two sub-periods further: the fragmentizing period and post-fragmentizing period. Accordingly, in practice, the process can be divided into three periods. The three periods are all involved in polymerization: 1) at $t < t_1$, the size of the macro-particle is basically unchanged and the polymerization process begins at the surface and in the pores of the micro-particle and a thicker and thicker layer of polymer forms all around the micro-particles. With the polymerization proceeding, the resistance of diffusion of monomer into macro-particle increases; 2) at $t_1 < t < t_2$, fragmentation starts at $t = t_1$ and ends (the polymer/catalyst particles are at complete fragmentation stage) at $t = t_2$, where a critical particle growth factor (C^*) is used to describe fragmentation. After the polymer layer has covered the particle completely, $C > C^*$, then the particle is considered to be locally fragmented and it is free to expand [11]; 3) at $t > t_2$, the macro-particle is at complete fragmentation stage. In addition, if the macro-particle void fraction is higher than the critical void fraction ($\varepsilon > \varepsilon^*$), the micro-particles extend freely to keep constant ε^*. Furthermore, the macro-particle consists of unfragmented core with the radius of R_C and outside $(n - 1)$ layers with constant spatial position for each layer in this work.

Under these points, a multi-layer CSM [12] is used to describe the macro-particle (see Figure 1b), and the whole polymer particle is handled as a reactor in the following mathematical modeling. It should be noted that the physical model employed is a revised MGM. Thus, the following mathematical model is based on the revised MGM.

Mathematical modeling

Here a further evolution of the revised MGM, from homo- to co-polymerization (preparing LCBPs) is

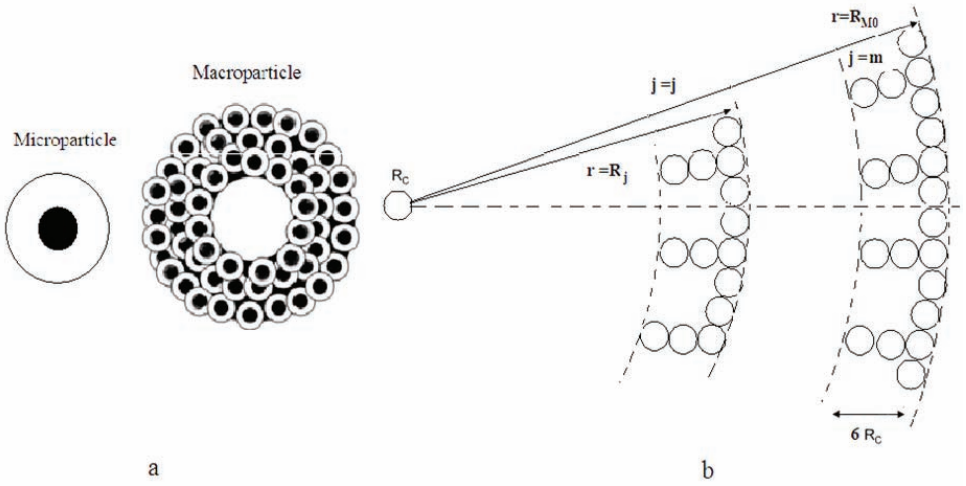

Figure 1. Schematic representation of physical model for polypropylene particle growth (a. physical model, b. micro-particle distribution within the initial macro-particle).

proposed. For the two types of polymerizations, the main difference of modeling is the polymerization rate equation, which will be described later. In addition, there are still some assumptions for the revised MGM: 1) the catalyst active-site concentration of each layer within the macro-particle is identical; 2) only diffusion between layers is considered; 3) the polymerization rate for each layer is calculated based on the average monomer concentration of each layer; 4) the average monomer concentration and temperature for each layer are used to calculate the volume for each sphere at a given interval. Following Figure 1 and using the hypotheses above, it is possible to write the governing equation (in dimensionless form) for the fragmented layer and unfragmented layer (solid-core) based on mass and heat balance equations.

For fragmented zone:

Mass balance:

$$\frac{\partial M}{\partial \tau}=\frac{1}{r^2}\frac{\partial}{\partial r}\left(r^2\frac{\partial M}{\partial r}\right)-\Phi^2\Re\frac{1-\varepsilon}{\varphi^3}\frac{1}{\varepsilon}^2\Re\frac{1-\varepsilon}{\varphi^3}\frac{1}{\varepsilon} \tag{1}$$

Heat balance:

$$\frac{\partial \theta}{\partial \tau}=Le\frac{1}{r^2}\frac{\partial}{\partial r}\left(r^2\frac{\partial M}{\partial r}\right)-\beta\Phi^2Le\Re\frac{1-\varepsilon}{\varphi^3}\frac{1-\varepsilon}{\varphi^3} \tag{2}$$

Boundary conditions:

$$r=1,\ \frac{\partial M}{\partial r}=Sh(1-M),\ \frac{\partial \theta}{\partial r}=Nu(1-\theta) \tag{3}$$

In addition, herein, we also consider the transition relations between the fragmented and unfragmented zones in the macro-particle as described in Eq. (4):

$$\left.\frac{\partial M}{\partial r}\right|_{r_m^+}=XD\left.\frac{\partial M}{\partial r}\right|_{r_m^-};\ \left.\frac{\partial \theta}{\partial r}\right|_{r_m^+}=\left.\frac{\partial \theta}{\partial r}\right|_{r_m^-} \tag{4}$$

For unfragmented zone:

Mass balance:

$$\frac{\partial M}{\partial \tau}=\frac{1}{r^2}\frac{\partial}{\partial r}\left(r^2\frac{\partial M}{\partial r}\right)-\Phi g^2\Re_g\frac{1}{\varepsilon} \tag{5}$$

Heat balance:

$$\frac{\partial \theta}{\partial \tau}=Le\frac{1}{r^2}\frac{\partial}{\partial r}\left(r^2\frac{\partial M}{\partial r}\right)-\beta\Phi^2Le\Re\frac{1-\varepsilon}{\varphi^3} \tag{6}$$

Boundary conditions:

$$r=0,\frac{\partial M}{\partial r}=0,\ \frac{\partial \theta}{\partial r}=0 \tag{7}$$

$$r=R_m/R_M,\frac{\partial M}{\partial r}=XDSh\left(1-M_m\right),\ \frac{\partial \theta}{\partial r}=Nu(1-\theta) \tag{8}$$

where m is the number of the outermost layer in the unfragmented zone.

Initial conditions:

$$\tau=0,\ M=0,\ \theta=1 \tag{9}$$

where

$$\Phi=(R_M^2((1-\varepsilon_0)m4\pi R_C^2\eta^*M_0)/(M_0D_l))^{\frac{1}{2}} \tag{10}$$

$$\Phi g=(m-1)/n/(XD^{\frac{1}{2}}),\ \ m=n,n-1,...,1 \tag{11}$$

In order to evaluate the deactivation of catalyst and the fragmentation of catalyst-containing particles, the single particle growth factor (C) is defined as:

$$C_j=\frac{R_s(r_M,t)}{R_C} \tag{12}$$

In addition, C^* is defined as the critical growth factor. When $C_j > C_j^*$, the jth layer is fragmented but its configuration is still unchanged. However, if $\varepsilon > \varepsilon^*$, the micro-particles extend freely to keep constant ε^*. Accordingly, for the unfragmented zone [20]:

$$\varepsilon\left(r_M,t\right)=1-\left(1-\varepsilon_0\right)\left[C\left(r_M,t\right)\right]^3 \tag{13}$$

$$R_j=6R_{C,j},\ \ j=1,...,n \tag{14}$$

and for the fragmented zone [20]:

$$\varepsilon\left(r_M,t\right)_{\text{zone}}=\varepsilon^* \tag{15}$$

$$R_j=\left\{\frac{\left(1-\varepsilon_0\right)}{\left(1-\varepsilon^*\right)}\left[6C_j\left(t\right)R_C\right]^3\left[j^3-\left(j-1\right)^3\right]+R_{j-1}^3\right\}^{\frac{1}{3}},\ \ j=j,...,n \tag{16}$$

Besides, when the m^{th} layer is at fragmented stage:

$$r_g=\frac{R_{j-1}}{R_M\left(t_0\right)}=\frac{j-1}{m} \tag{17}$$

The dimensionless polymerization rate for each layer within the macro-particle can be calculated as follows [20,13,27]:

For SiO_2-supported metallocene catalyst [13]:

$$\Re_j=\exp\left(-\frac{E_a}{R_{\text{gas}}T_0}\left(\frac{1}{\theta_j}-1\right)\right)Cx_jM_{C,j} \tag{18}$$

and for SiO_2-supported dual function metallocene catalyst [27]:

$$\Re_j = \frac{(K_{P0}^1 \exp(-E_{A1}/(R_{gas}\theta_j))Cx_1 + K_{P0}^2 \exp(-E_{A2}/(R_{gas}\theta_j))Cx_2)M_{c,j}}{(K_{P0}^1 \exp(-E_{A1}/(R_{gas}T_0))Cx_1 + K_{P0}^2 \exp(-E_{A2}/(R_{gas}T_0))Cx_2)M_0} \quad (19)$$

Using a quasi-steady state assumption for micro-particle, the following equations can be obtained [28]:

$$\frac{d\varphi_j}{dt} = \frac{k_p M_n}{3R_C \rho_{PP} \varphi_j^2} M_{C,j} M_0 \quad (20)$$

$$M_{C,j} = \frac{\eta^* M_j}{1 + \frac{1}{3}\frac{R_C^2}{D_C} k_e (1 - 1/\varphi_j)} \quad (21)$$

While the interval ($\Delta t = t_2 - t_1$) approaching 0, the following equation can be obtained:

$$\varphi_j(t_2) = (\varphi_j^3(t_1) + \frac{0.001 k_p Cx_0 \rho_{Cat} M_n \Delta t}{R_C \rho_{PP}} \frac{1}{2}(M_{C,j}(t_1) + M_{C,j}(t_2))M_0)^{1/3} \quad (22)$$

In addition, the temperature gradient can be obtained using the following equation [29]:

$$\theta_C - \theta_j = (-\Delta H_p) D_C / (k_e T_0) \times \times \left(1 + \frac{R_C^2}{3D_C}(1 - \frac{1}{C(i,j)}) k_p Cx_j Cx_0 \rho_{Cat}\right) \quad (23)$$

Solution method and particle parameter values

The revised MGM, *i.e.*, Eqs. (1)-(23) are solved to obtain the intraparticle flow fields in propylene polymerization with SiO_2-supported metallocene catalyst and dual function metallocene catalyst to prepare homopolypropylene and LCBP. To calculate the flow field in a growth polymer particle, Eqs. (1)-(23) are numerically implemented as a Matlab User-Defined-Function and are solved with a chasing method.

In the following analysis, the simulated results depend on the input valuses of the parameters presented in Eqs. (1)-(23). In the present work, the parameters include the physical and transport properties of the reaction mixture and the kinetic rate constants. Many researchers [5-34] have studied olefin polymerization including propylene polymerization with SiO_2-supported metallocene catalyst and dual function metallocene catalyst to prepare homopolypropylene and LCBP. A set of reference values of these parameters are selected and listed in Tables 1 and 2. Unless noted otherwise, the values used for the simulation are those listed in Tables 1 and 2.

Table 1. Major parameters for the homopolymerization system

Parameter	Value at 80 °C	Reference
M_0	1450	30
ΔH_p	8.37×10^4	18,30
E_a	6.07×10^4	30
k_P	2.640	31
M_n	0.042	/
D_l	2.24×10^{-10}	18
D_s	1×10^{-11}	18
k_s	3.58×10^{-9}	18
C_p	1920	30
h	744	30
k_e	1.965	32
R_{gas}	8.318	/
ρ_{cat}	2260	30
ρ_{PP}	910	18, 28, 30
C_{x0}	1	28
R_C	6×10^{-9}	32
R_{M0}	4.5×10^{-5}	32
ε_0	0.825	32
ε^*	0.4	32
n	1250	32
φ^*	1.1	32

RESULTS AND DISCUSSION

As described above, this work concentrates on the modeling comparison between intraparticle transports during propylene polymerizations using supported metallocene and dual function metallocene catalysts. The intraparticle transport effect is described *via* intraparticle monomer concentration, temperature, and polymerization rate. In addition, some other variables linking to intraparticle flow field, such as macro-particle void fraction, micro-particle growth factor, and catalyst concentration of active center are also used to describe the intraparticle transport effect.

Intraparticle mass transfer phenomenon

In a propylene polymerization system, polymerization occurs within catalyst/polymer particles (*i.e.*, intraparticle active sites) and monomer should enter the particles by diffusion first. It means that polymerization is a couple of diffusion and reaction in nature. For diffusion, many intraparticle parameters, such as macro-particle void fraction, micro-particle increase factor, catalyst concentration, polymerization time, etc., can influence the intraparticle monomer concentration distribution. They will be predicted and dis-

cussed based on the proposed models. Figure 2 illustrates the distributions of monomer within the macro-particle at different polymerization time for two polymerization systems.

Table 2. Major parameters for the copolymerization system

Parameter	Value at 80 °C	Reference
M_0	1450	30
ΔH_p	1.066×10^5	14
E_a^1	3.377×10^4	33
E_a^2	4.39×10^4	31
k_P^1	14.3	5,33
k_P^2	2.64	29,31,34
M_n	0.042	/
D_l	2.24×10^{-10}	18
D_s	1×10^{-11}	18
k_s	3.58×10^{-9}	18
C_p	1920	19
h	744	19
k_e	1.965	32
R_{gas}	8.318	/
ρ_{PP}	900	18,28,30
ρ_{cat1}	2480	5,33
ρ_{cat2}	2260	28,30
C_{x01}	0.5	28
C_{x02}	0.5	28
R_C	6×10^{-9}	32
R_{M0}	4.5×10^{-5}	32
φ^*	1.1	32
n	1250	32
ε_0	0.825	32
ε^*	0.4	32

From Figure 2, one can see that there are similar monomer distributions for the two studied systems. Figure 2 also shows that the monomer concentrations are higher at the surface than that within the macro-particle. Furthermore, Figure 2 indicates that there are peak distributions for the two systems and their positions are different. The positions are at 2 and 10 s for the homopolymerization and copolymerization systems for preparing linear polypropylene and LCBP, respectively. Since the position, the monomer concentration gradually increases with the polymerization proceeding for any system. For the whole polymerization process, the appearance of peak distribution implies that monomer distribution is the coupling effect of reaction and diffusion, but not a single effect of reaction or diffusion. At the initial stage of polymerization, diffusion rate is high and reaction is the controlling-step, which leads to the increase in monomer concentration. With the polymerization proceeding, the resultant polymers fill within the particles to block the pores within the particles, thus the diffusion resistance increases. The controlling-step can change from reaction to diffusion due to the increase in diffusion resistance. In addition, as described above, catalyst/polymer particles fragmentize shell-by-shell towards the core of the particles due to the hydraulic force resulted from polymerization within the pores, which leads to the decrease in mass transfer resistance and increase in intraparticle monomer concentration (*i.e.*, at each layer of particle). In order to further describe the intraparticle mass transfer, the monomer distributions of each layer within the macro-particle for the two systems are also simulated and the results are shown in Figure 3.

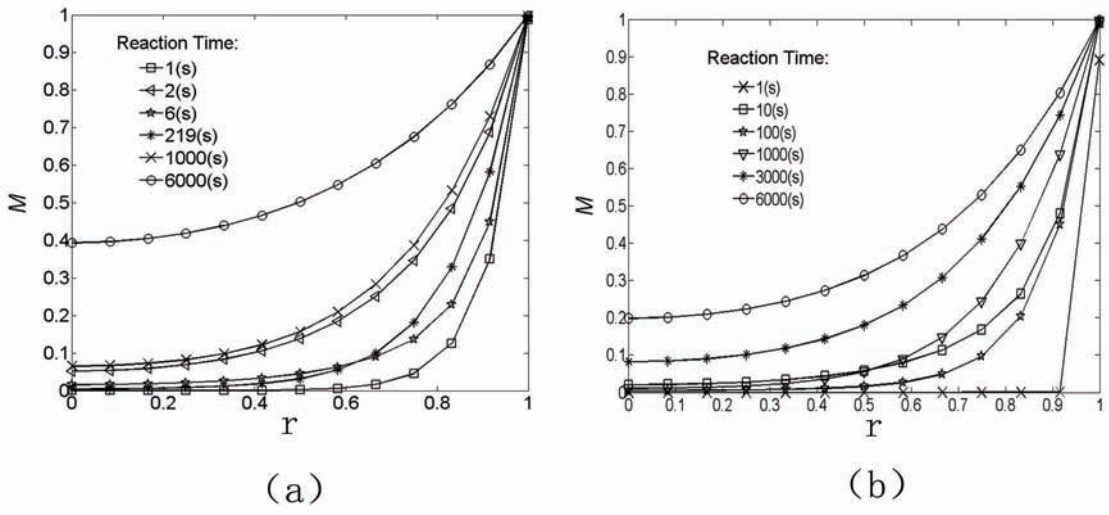

Figure 2. Radial profiles of propylene concentration in macro-particle (a. the homopolymerization system; b. the copolymerization system).

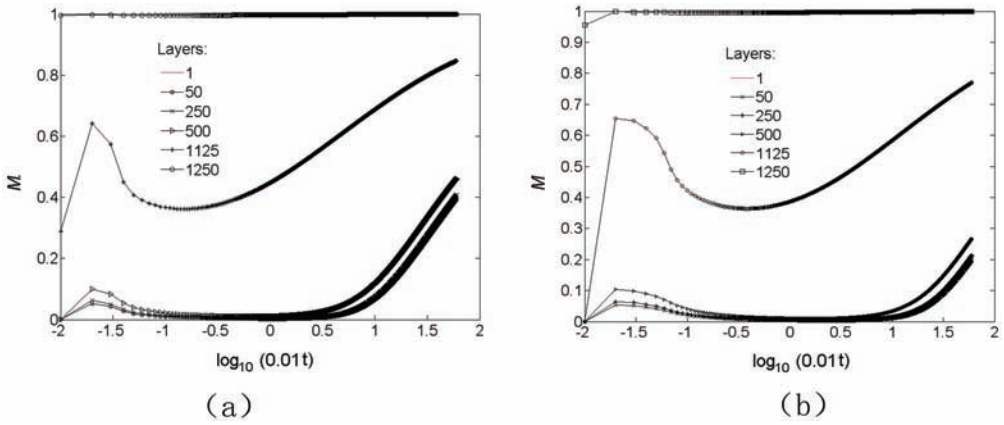

Figure 3. Propylene concentration distributions along different layers in macro-particle (a. the homopolymerization system; b. the copolymerization system).

From Figure 3, one can see that that the distributions for the two systems are similar. The change in monomer concentration within the macro-particle is complicated. The monomer concentration of each layer first increases, then decreases to a minimum value, and increases again during the polymerization processing. However, the variation of monomer concentration near the outermost layer is very small as shown in Figure 3. The first increase in monomer concentration of each layer is due to the monomer diffusion. After that, the diffusion rate decreases because the resultant polymers fill within the particles and block the pores within the particles. Furthermore, as described above, the catalyst/polymer particles fragmentize in shell-by-shell manner, resulting in decrease in mass transfer resistance and increase in intraparticle monomer concentration. Based on the above discussions, it is easy to conclude that the camel profiles shown in Figure 3 are the reason of sequence inversion phenomenon shown in Figure 2. On the other hand, despite the similar profiles for the two systems as shown in Figures 2 and 3, one can find that there are still some differences between the two systems. For instance, for the homopolymerization system, the first max monomer concentration position is at 2 s, the innermost layer within the macro-particle begins to fragmentize at 6 s, and the macro-particle grows rapidly at 219 s. However, for the copolymerization system, the positions are at 2, 14 and 573 s, respectively. It means that the two types of catalyst particle kinetics are different in nature.

Figures 2 and 3 prove that the whole process is complicated and any change in the process can be explained by the coupling effect of reaction and diffusion or the micro-particle growth and macro-particle fragmentation, which combines many intraparticle parameters as described above and will be discussed as follows. We also calculated the micro-particle growth factor and the macro-particle mean void fraction using the proposed models, which are shown in Figures 4 and 5, respectively.

From Figure 4, one can see that the intraparticle

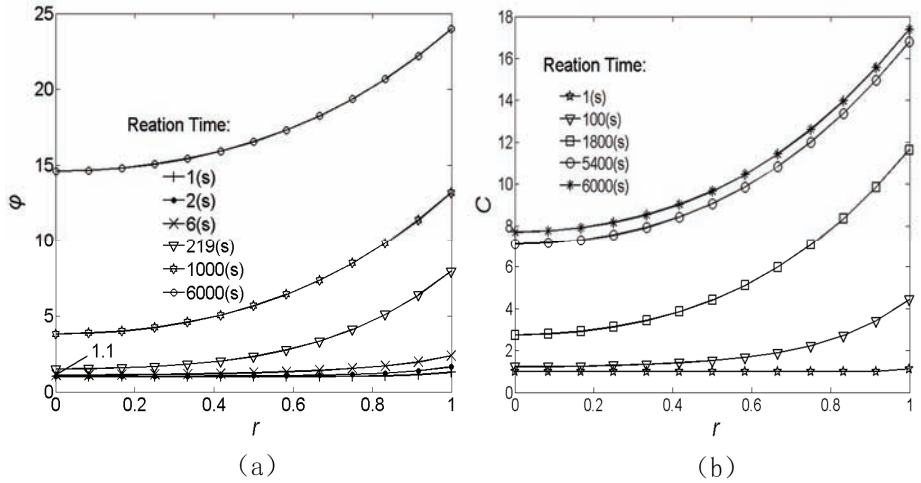

Figure 4. Micro-particle growth factor profiles (a. the homopolymerization system; b. the copolymerization system).

growth factor distributions for the two studied systems are similar. In addition, the growth factor of each layer increases with the polymerization proceeding. By comparing the radius of micro-particle at the outermost layer with that at the innermost layer, one can see that their differences are 64.16 and 125.7 for the homopolymerization and copolymerization systems for preparing linear polypropylene and LCBP, respectively. It means that the penetration performances for the two types of catalyst particles are excellent. From Figure 5, one can observe obviously that the macro-particle mean void fractions decrease to 0.4 at 219 and 573 s for the homopolymerization and copolymerization systems, respectively. After that, the mean void fractions for the two systems are almost constant. The above simulation result regarding the mean void fraction is the same as that reported by Diana *et al*. [20]. Furthermore, the active catalyst-center concentrations of each layer for the two systems are predicted using the models proposed and the results are shown in Figure 6.

Figure 6 illustrates that the intraparticle active catalyst-center concentration profiles are similar for the two studied systems, and the concentrations for the two studied systems all decrease slowly. The extent of decrease for the two systems is very low. Thus, the current results prove that the decrease in active catalyst-center concentration can be ignored, which is the same as that reported in the literature [16–18,20].

Intraparticle heat transfer phenomenon

Figure 7 describes the temperature distributions of each layer within the macro-particle for the two systems.

From Figure 7, one can see that the temperature distributions for the two systems are similar. The intraparticle temperature gradients increase with polymerization proceeding. However, the variation of temperature gradient is very small for both of them. For

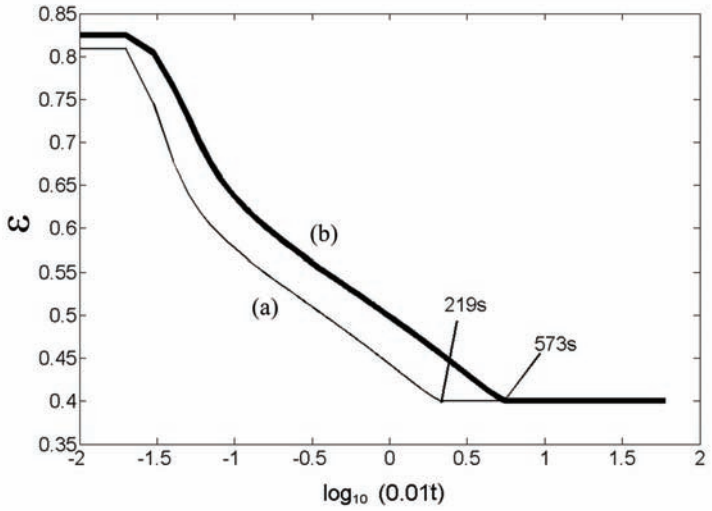

Figure 5. Macro-particle mean void fraction profiles (a. the homopolymerization system; b. the copolymerization system).

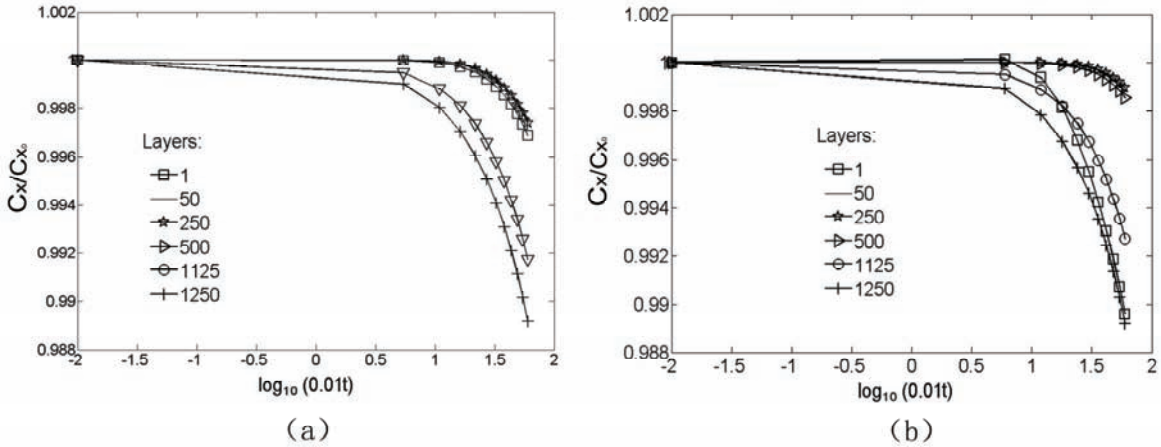

Figure 6. Active site concentration profiles within macro-particle (a. the homopolymerization system; b. the copolymerization system).

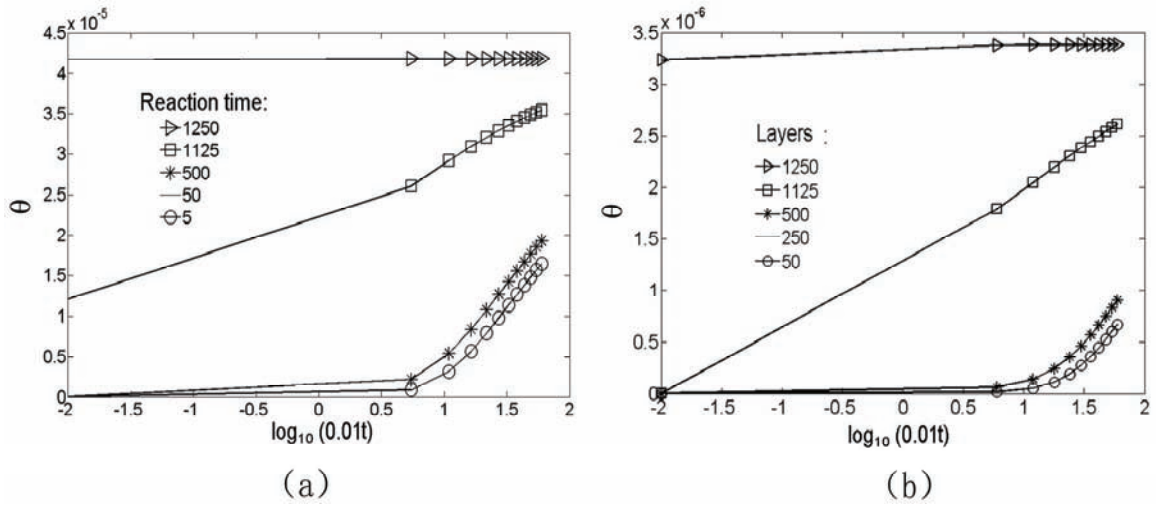

Figure 7. Intraparticle temperature distribution profiles (a. the homopolymerization system; b. the copolymerization system).

instance, the changed orders of magnitude are 10^{-5} and 10^{-6} for the homopolymerization and copolymerization systems, respectively. In addition, comparing Figure 7 with Figure 3, the temperature distributions are also very similar to the monomer concentration distribution. It implies that these changes are influenced by the polymerization heat.

On the other hand, the mean temperatures within the macro-particle are also predicted using the same models. The predicted mean temperature profiles for the two systems are shown in Figure 8.

Figure 8 shows that the varying temperature gradients are very small for the two systems. In addition, one can see from Figure 8 that the average temperature for the copolymerization system is higher than that for the homopolymerization system, which is due to higher reaction heat as a result of higher polymerization rate for the copolymerization system as illustrated in Figure 9.

It means that higher reaction rate leads to higher reaction heat, and higher reaction heat leads to more significant influence on the intraparticle heat transfer. Nevertheless, the low intraparticle temperature gradient obtained for the two systems suggests that the intraparticle heat transfer resistance can be ignored in the case of propylene polymerization.

Polymerization rate profile

As described above, the intraparticle transfer is influenced by the polymerization rate. Herein, the polymerization rate profiles for the two systems are also simulated and the results are shown in Figure 9.

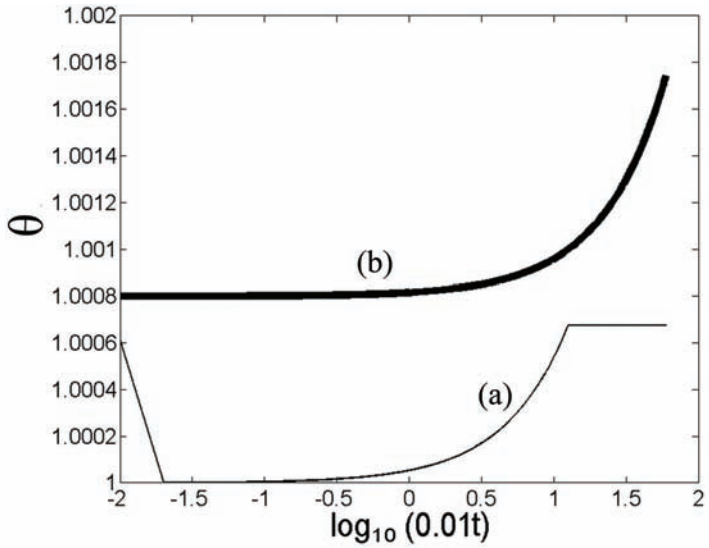

Figure 8. Intraparticle mean temperature distribution profiles.

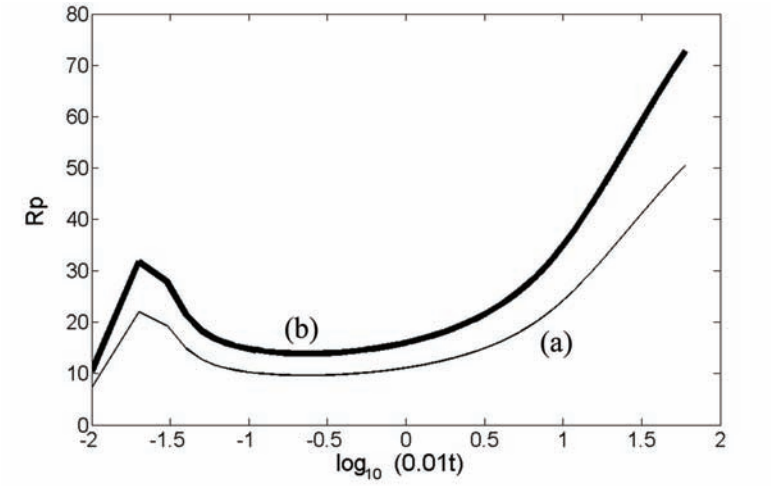

Figure 9. Polymerization reaction rate profiles.

From Figure 9, one can see that the polymerization rate profiles for the two systems are similar and also complicated. During the polymerization, the rates increase quickly to the maximum values and then decrease to the minimum values. After that, the rates increase again. At the start of polymerization, the catalyst particles are instantly activated, so the polymerization rate increases quickly at this stage. As the polymerization proceeding, the pores in the catalyst-containing particles are filled with and blocked by the obtained polymers, which results in the increase in monomer diffusion resistance to intraparticle active center. The polymerization rate decreases subsequently. On the other hand, the high hydraulic force as a result of polymerization within the pores causes shell-by-shell fragmentation from the surface to centre, new catalyst active centers appear in turn. Thus, the polymerization rate increases again.

The result obtained in this work regarding the polymerization rate is similar to that reported in Ref. [11]. As a matter of fact, the variation of total polymerization rate reflects the change in the radius of macro-particle and their correlation is linear.

CONCLUSIONS

In this paper, two improved MGMs are suggested to describe propylene polymerization with silica-supported metallocene catalyst and dual function metallocene catalyst to homopolypropylene and LCBP. The intraparticle flow fields described via intraparticle monomer concentration, temperature, and polymerization rate involved in polymerizations are predicted. The simulation results show that the two flow field distributions involved are basically identical. The simulation results also show that both the two polymerization processes have an initiation stage and the controlling step is reaction-diffusion-reaction with the polymerization proceeding. Furthermore, the simulation results show that the intraparticle mass transfer resistance has significant effect on the polymerization, but the heat transfer resistance can be ignored.

Acknowledgements

The authors gratefully acknowledge financial support from the National Natural Science Foundation of China (No. 21076171), and the State-Key Laboratory of Chemical Engineering of Tsinghua University (No. SKL-ChE-10A03). The authors also thank the anonymous referees for the comments on this manuscript.

Nomenclature

C_p	heat capacity of the polymer particle, J kg^{-1} K^{-1}
C_{x_0}	active site concentration at t = 0, mol·kg^{-1}
C_x	active site concentration, mol kg^{-1}
D_1	diffusion coefficient in macro-particle, m^2 s^{-1}
D_C	diffusion coefficient in micro-particle, m^2 s^{-1}
E_a	activation energy, J mol^{-1}
h	heat transfer coefficient in external film, J m^2 s^{-1} K^{-1}
j	the jth layer of single particle
k_P	polymerization rate constant, m s^{-1}
k_e	intraparticle heat transfer coefficient, W m K^{-1}
k_C	intraparticle mass transfer coefficient, m^2 s^{-1}
Le	Lewis number
M_n	propylene mole mass, kg mol^{-1}
M	propylene concentration within macro-particle
M_c	propylene concentration at active site, mol m^{-3}
M_0	propylene concentration in the bulk, mol m^{-3}
m	the mth layer
n	total layers in single particle
Nu	Nusselt number
R_P	propylene polymerization rate, mol m^{-3} s^{-1}

R particle radius, m
R_C micro-particle radius at t=0, m
R_{ga} gas constant, $J \cdot mol^{-1} \cdot K^{-1}$
R_M radius of the outside layer within the macro-particle, m
r_g dimensionless radius of the unfragment part within the macro-particle
r dimensionless radius
Sh Sherwood number
T temperature, K
T_0 temperature at $t = 0$, K
t polymerization time, s
V volume, m^3
XD diffusion coefficient ratio of macro-particle fragment before to after
β Prater constant
ε void fraction
ε^* critical void fraction
ε_0 initial void fraction
ΔH polymerization reaction heat, $J \cdot mol^{-1}$
ρ_{cat} active site density, $kg \cdot m^{-3}$
ρ_{pp} macro-particle density, $kg \cdot m^{-3}$
$\Re$ dimensionless polymerization rate
Δt polymerization time interval, s
τ dimensionless polymerization time
$\Delta\tau$ dimensionless polymerization time interval
η^* adsorption constant
θ dimensionless temperature
Φ Thiele constant

Subscripts

0 initial stage
c micro-particle
g solid core
i the ith time
j the jth layer
l macro-particle
p propylene monomer
PP polypropylene

REFERENCES

[1] X.J. Zheng, M. Smit, J.C. Chadwick, J. Loos, Macromolecules **38** (2005) 4673-4678

[2] P.D. Iedema, M. Wulkow, H.C.J. Hoefsloot, Macromolecules **33** (2000) 7173-7184

[3] I.M. Maafa, J.B.P. Soares, A. Elkamel, Macromol. React. Eng. **1** (2007) 364-383

[4] J.B.P. Soares, Macromol. Mater. Eng. **12** (2003) 70-87

[5] H. Yiannoulakis, A. Yiagopoulos, P. Pladis, C. Kiparissidis, Macromolecules **33** (2000) 2757-2766

[6] S. Mehdiabadi, J.B.P. Soares, A.H. Dekmezian, Macromol. React. Eng. **2** (2008) 37-57

[7] L.C. Simon, J.B.P. Soares, Macromol. Theory Simul. **11** (2002) 222-232

[8] R. Duchateau, Chem. Rev. **102** (2002) 3525-3542

[9] G.G. Hlatky, Chem. Rev. **100** (2000) 1347-1376

[10] T.F. McKenna, J.B.P. Soares, Chem. Eng. Sci. **56** (2001) 3931-3949

[11] G. Fink, B. Steinmetz, J. Zechlin, C. Przybylac, B. Tesche, Chem. Rev. **100** (2000) 1377-1390

[12] W.R. Schmeal, J.R. Street, AIChE J. **17** (1971) 1189--1197

[13] R. Galvan, M. Tirrell, Comput. Chem. Eng. **10** (1986) 77-85

[14] R.A. Hutchinson, C.M. Chen, W.H. Ray, J. Appl. Polym. Sci. **44** (1992) 1389-1416

[15] Y. Chen, X. G. Liu, Polymer **46** (2005) 9434-9442

[16] F. Bonini, V. Fraaije, G. Fink, J. Polym. Sci., A **33** (1995) 2393-2402

[17] A. Alexiadis, C. Andes, D. Ferrari, F. Korber, K. Hauschild, M. Bochmann, G. Fink, Macromol. Mater. Eng. **289** (2004) 457-466

[18] A. Alexiadis, C. Andes, Appl. Math. Model. **32** (2008) 99--111

[19] M.A. Ferrero, M.G. Chiovetta, Polym. Eng. Sci. **27** (1987) 1436-1447

[20] A. Diana, M.G.C. Estenoz, J. Appl. Polym. Sci. **81** (2001) 285-311

[21] C. Przybyla, B. Weimann, G. Fink, Influence of the particle size of silica supporton the kinetic and the resulting polymer properties at the polypropylene polymerization with heterogeneous metallocene catalyst Part II: Development of a model as well as a mathematical simulation, in: W. Kaminsky (Ed.), Metallorganic Catalysts for Synthesis and Polymerization, Springer, Berlin, 1999, pp. 333-346

[22] J. Zechlin, B. Steinmetz, B, Tesche, G. Fink, Macromol. Chem. Phys. **201** (2000) 515-524

[23] E.J. Nagel, V.A. Kirillov, W. Harmon Ray, Ind. Eng. Chem. Prod. Res. Dev. **19** (1980) 372-381

[24] H.R. Li, Z.H. Luo, J. Chem. Eng. Chin. Univ. **25** (2011) 423-429 (In Chinese)

[25] J.J. Han, H.W. Lee, W.J. Yoon, K.Y. Choi, Polymer **48** (2007) 6519-6531

[26] J.B.P. Soares, A.E. Hamielec, Polym. React. Eng. **3** (1995) 261-324

[27] H.R. Li, Master Dissertation, Xiamen University, Xiamen, 2010 (in Chinese)

[28] X. G. Liu, Chin J. Chem. Eng. **15** (2007) 545-553

[29] S. Floyd, K.Y. Chio, T.W. Taylor, J. Appl. Polym. Sci. **32** (1986) 2935-2960

[30] C.W. James, R.S. Chien, J. Polym. Sci., A **29** (1991) 459--470

[31] G.B. Meier, G. Weickert, W.P.M. Van Swaaij, J. Polym. Sci., A **39** (2001) 500-513

[32] C.M. James, B.P.W. Chien, J. Polym. Sci., Aolym. Chem. **28** (1990) 15-38

[33] A. Krallis, C. Kiparissides, Chem. Eng. Sci. **62** (2007) 5304-5311

[34] S. Floyd, K.Y. Chio, T.W. Taylor, J. Appl. Poly. Sci. **33** (1987) 1021-1065.

HUA-RONG LI[1]
LIMING CHE[1]
ZHENG-HONG LUO[1,2]

[1]Department of Chemical and Biochemical Engineering, Xiamen University, Xiamen, China
[2]Department of Chemical Engineering, Shanghai Jiao Tong University, Shanghai, China

NAUČNI RAD

MODELOVANJE INTRAPARTIKULARNIH PRENOSA TOKOM POLIMERIZACIJA PROPILENA PRIMENOM NANEŠENIH METALOCENA I METALOCENA SA DVOSTRUKOM FUNKCIJOM KAO KATALIZATORA: MODEL ČESTICE

U ovom radu su opisana dva poboljšana multizrnasta modela (MGM) za pripremu homopolipropilena i dugo-lančanog razgranatog polipropilena dobijenih polimerizacijom propilena, pomoću metalocena nanetih na siliki ili metalocena sa dvostrukom funkcijom kao katalizatora. Prikazani modeli se koriste za predviđanje intrapartikularnih polja strujanja uključena u polimerizaciju. Rezultati simulacije pokazuju da su raspodele polja strujanja u osnovi identične. Rezultati pokazuju, takođe, da oba polimerizaciona procesa imaju fazu inicijacije i da je kontrolišući stupanj kod oba proseca reakcija-difuzija-reakcija sa napredovanjem polimerizacije. Osim toga, rezultati simulacije pokazuju da otpor intrapartikularnog prenosa mase ima značajan uticaj na polimerizaciju, dok se otpor prenosa toplote može zanemariti.

Ključne reči: metalocen nanešen na siliki, metalocen dvostruke funkcije nanešen na siliki, fragmentacija "ljuska po ljuska", polimerizacija propilena, dugo-lančani i razgranati poliolefini, model rasta čestice.